Available online at www.sciencedirect.com
ScienceDirect
Bioelectrochemistry 70 (2007) 205–213
Bioelectrochemistry
www.elsevier.com/locate/bioelechem

# Electrochemical screening of anti-microbial peptide LL-37 interaction with phospholipids

Frances Neville [a], David Gidalevitz [b], Girish Kale [a], Andrew Nelson [c,*]

[a] Institute for Materials Research, School of Process, Environmental and Materials Engineering, University of Leeds, LS2 9JT, UK
[b] Department of Chemical Engineering, Illinois Institute of Technology, Chicago, IL 60616, USA
[c] Center for Self Organising Molecular Systems, School of Chemistry, University of Leeds, LS2 9JT, UK

Received 10 April 2006; received in revised form 18 May 2006; accepted 7 July 2006
Available online 12 July 2006

**Abstract**

LL-37 is an α-helical antimicrobial peptide of human origin. It is a 37 residue cathelicidin peptide. This paper explores the use of electrochemical methods to investigate the interaction of LL-37 with phospholipid and lipid A monolayers on a mercury drop electrode. Experiments were carried out in Dulbecco's phosphate buffered saline at pH ~7.6. The capacity-potential curves of the coated electrode in the presence and absence of LL-37 were measured using out-of-phase *ac* voltammetry. The frequency dependence of the complex impedance of the coated electrode in the presence and absence of LL-37 was estimated at −0.4 V versus Ag/AgCl 3.5 mol $dm^{-3}$ KCl. The monolayer permeability to ions was studied by following the reduction of Tl(I) to Tl(Hg) at the coated electrode. LL-37 shows no significant interaction with DOPC. However, LL-37 shows a small interaction with DOPG and lipid A within a DOPC monolayer where the monolayer permeability is marginally increased and the zero frequency capacitance (ZFC) is marginally decreased in both cases. LL-37 shows a significant interaction with a lipid A monolayer thereby decreasing the ZFC by 30%. The results concur with the known membrane active properties of LL-37 and establish this electrochemical approach as a key technique for screening peptides.


*Keywords:* Antimicrobial; LL-37; Phospholipid; Lipid A; Impedance; Mercury

## 1. Introduction

Antimicrobial defence systems are required on a daily basis in nature as animals and plants are constantly under attack by harmful agents such as bacteria and viruses. There are fewer numbers of bacterial infections that can be treated by prescribed antibiotic medicines as a result of the number of multi-drug resistant bacteria increasing worldwide [1–7]. The development of a new class of antibiotic is of prevalent need today. Antimicrobial peptides are part of the innate immune system and have the ability to fight infection [8,9]. It has been demonstrated that some antimicrobial peptides are able to differentiate between types of cells due the membranes being of different lipid compositions [10–12]. This property allows antimicrobial peptides to disrupt bacterial membranes whilst leaving eukaryotic plasma membranes unaltered. These properties make antimicrobial peptides and their mimics great potential therapeutic agents and viable alternatives to conventional antibiotic drugs. However, one of the major drawbacks in designing pharmaceutical antimicrobial peptides and peptide mimics is the lack of a molecular level understanding of their interactions with membrane lipids and mechanism of action.

Eukaryotic and bacterial membranes are composed of different lipid components, with the former comprising mainly of phosphatidylcholine (PC), sphingomyelin and cholesterol, whereas the latter contains substantial amounts of negatively charged phospholipids, such as phosphatidylglycerol (PG), cardiolipin or lipopolysaccharides (LPS). This work models the outer leaflet of the human red blood cell (RBC) membrane and different layers of the Gram-positive and Gram-negative bacterial outer cell membranes with a monolayer composed of phospholipid molecules at the mercury solution interface. Zwitterionic dioleoyl phophatidylcholine (DOPC) is used to simulate the RBC and negatively charged dioleoyl phosphatidylglycerol (DOPG) and lipid A are used to imitate the external

* Corresponding author. Tel.: +44 113 6409; fax: +44 113 6452.
*E-mail address:* andrewn@chem.leeds.ac.uk (A. Nelson).

1567-5394/$ - see front matter © 2006 Elsevier B.V. All rights reserved.
doi:10.1016/j.bioelechem.2006.07.006

layer of the bacterial membrane. Lipid A is a major component of lipopolysaccharides isolated from the *E. coli* outer cell membrane. In this paper, membrane interactions of LL-37, the only human α-helical antimicrobial peptide from the cathelicidin family, are studied. LL-37 (LLGDFFRKSKEKIGKEFKRIVQ RIKDFLRNLVPRTES [13]) is composed of 37 amino acid residues and was originally isolated from neutrophil-specific granules but is also found at the mucosal linings in the body and skin [14,15]. LL-37 has been found to have antimicrobial properties [16–18] as well as having other abilities relating to the innate immune system such as induction or modulation of chemokine and cytokine production and inhibition of proinflammatory responses of host cells to bacterial components [19].

This study was carried out to specifically look at the applicability of electrochemical techniques including electrochemical impedance spectroscopy to investigate the interaction of LL-37 with phospholipid monolayer coated electrodes. Electrochemical techniques have been applied to study lipid–peptide interactions only relatively recently [20–24]. Research has mainly been carried out on the phospholipid dioleyl phosphatidylcholine (DOPC) and the pore-forming peptide gramicidin A [20,21,23–25]. The aim of this study is to probe the question of LL-37 selectivity between prokaryotic and eukaryotic cells and to assess whether these techniques form a scientific basis for the development of routine screening systems for membrane active peptides.

## 2. Experimental

### 2.1. Apparatus and materials

Two distinct measurements were carried out using the electrochemical apparatus. The first series of measurements focused on impedance measurements in which no Faradaic process is involved. These experiments concentrated on capacitive elements [21,25,26]. The second series investigated the transport of $Tl^+$ ions in which a Faradaic process is involved [20]. The rationale for using $Tl^+$ as a probe is the following: (1) $Tl^+$ is isoelectronic with $K^+$ and thus is an effective probe for this ion's behaviour and the alkali metal ions in general [23]. (2) $Tl^+$ undergoes a rapid reversible redox reaction on the mercury surface with a reduction potential at about −0.42 V vs Ag/AgCl, 3.5 mol $dm^{-3}$ KCl, which is in the potential domain of the low capacity and ion impermeable region of the DOPC monolayer [23]. As a consequence, in the presence of the DOPC monolayer the electrochemical reduction of $Tl^+$ is suppressed because $Tl^+$ is denied access to the mercury surface. When the DOPC monolayer becomes permeable a reduction current of $Tl^+$ is observed. The results of both impedance and voltammetric measurements are considered in the analysis of the properties of the phospholipid and peptide modified phospholipid monolayer.

An Autolab PGSTAT 30 interface (Ecochemie, Utrecht, Netherlands) was used to measure capacitance–potential curves of the coated electrodes. An Autolab system, FRA and PGSTAT 30, controlled with Autolab software, was used in all the impedance versus frequency measurements of the coated electrodes. The PGSTAT 30 connected to a MacLab acquisition board and software (AD Instruments Ltd) was used in the sampled current voltammetry experiments to measure the reduction of $Tl^+$. The experiments were performed in a standard three electrode cell. An Ag/AgCl, 3.5 mol $dm^{-3}$ KCl reference electrode, with a porous sintered glass frit separating the 3.5 mol $dm^{-3}$ KCl solution from the electrolyte served as reference, and a platinum bar served as a counter electrode. The electrodes were located on either side of the working electrode respectively. All potentials are quoted in this paper versus the Ag/AgCl, 3.5 mol $dm^{-3}$ KCl reference electrode. In the impedance–frequency measurements, a solution resistance of around 280–300 Ω was recorded for the cell [25,26]. Diagnostic plots of the impedance data showed it to be that of an RC series circuit as before [25,26]. There was a distinct absence of instability at high frequencies and for this reason, the use of a fourth pseudo reference electrode was not considered necessary at this stage.

The electrolyte was Dulbecco's phosphate buffered saline (Invitrogen Life Technologies) and was used as supplied (1X solution). A blanket of argon gas was maintained above the fully deaerated electrolyte during all experiments. Monolayers of DOPC, DOPC+DOPG, DOPC+lipid A and lipid A were prepared as described earlier [25,26]. DOPC monolayers were formed after initially spreading 13 μ$dm^3$ of a 2 g $dm^{-3}$ solution of DOPC in pentane (HPLC grade, Fisher Scientific Chemicals Ltd) at the argon-electrolyte interface in the electrochemical cell [25–27]. The working solution of DOPC was obtained by dilution of the 50 g $dm^{-3}$ stock solution (Avanti Lipids). A 2 g $dm^{-3}$ solution of DOPG (Avanti Lipids) in chloroform (HPLC grade) was prepared. The DOPC+DOPG monolayer was obtained using a 1:1 v/v mixture of 2 g $dm^{-3}$ DOPC in pentane and 2 g $dm^{-3}$ DOPG in chloroform. Lipid A ((diphosphoryl, from *E.coli* F583), Sigma–Aldrich) was prepared in a 74:23:3 v/v% solvent of chloroform, methanol and water respectively. High grade solvents and 18.2 MΩ MilliQ water (Millipore) were used. The concentration of the lipid A working solution was 0.2 g $dm^{-3}$ and 300 μ$dm^3$ was spread onto the surface of the electrolyte in order to obtain a fivefold excess as is the case with all the lipids used. A 70:30 mol:mol DOPC+lipid A solution was prepared using the stock solutions of lipid A and DOPC. 15 μ$dm^3$ of this solution was spread onto the electrolyte surface. A fresh mercury drop (area, $A = 8.8 \times 10^{-7}$ $m^2$) was coated with the spread phospholipid layer [25,26] at the argon-electrolyte interface prior to each series of experiments to give a monolayer coated electrode.

The LL-37 peptide (Pepceuticals Ltd) solution was made up in 0.01% v/v acetic acid using 18.2 MΩ MilliQ water and 99% pure acetic acid (Sigma–Aldrich). A stock solution of $4.5 \times 10^{-5}$ mol $dm^{-3}$ LL-37 in acetic acid was further diluted to give a working solution of $2.2 \times 10^{-6}$ mol $dm^{-3}$ and this was used for injection under the lipid layer in the electrochemical cell. The final concentration of LL-37 peptide used was 8.9 nmol $dm^{-3}$ for all experiments. Aliquots of the LL-37 peptide working solution were injected below the layer into the electrolyte. The solution was then gently stirred for 5 min. Following this the phospholipid monolayer was deposited on the electrode. Such layers in this study are referred to as peptide modified layers regardless of the extent of interaction. In the experiments studying the Tl(I)/Tl(Hg) reduction, $TlNO_3$

(Sigma Products) was employed to prepare the stock solution (0.1 mol $dm^{-3}$) from which aliquots were added to the electrolyte.

### 2.2. Electrochemical impedance

Measurements of capacity versus potential for the coated electrode were carried out by measuring the out-of-phase current ($I''$) at potentials between −0.2 and −1.3 V vs Ag/AgCl at a frequency ($f$) of 75 Hz with 0.005 V rms ($\Delta V$) using the *ac* voltammetric method. Capacitance ($C_d$) was calculated from the $I''$ value using the equation $C_d=(I''/A\ \Delta V\omega)$ where $\omega$ is the angular frequency ($=2\pi f$) assuming RC series behaviour of the cell [26]. The capacitance–potential curve of the lipid coated electrode was recorded prior to each experiment. At least two capacitance–potential curves following respective depositions on a fresh electrode surface were recorded for the individual peptide–phospholipid interactions.

Measurements of the impedance ($Z$) versus frequency of the electrode systems using frequencies logarithmically distributed from 65,000 to 0.1 Hz, 0.005 V rms at potentials of −0.4 V vs Ag/AgCl were carried out on the coated electrode systems. The impedance versus frequency plot of the lipid coated electrode was recorded prior to each experiment. At least three impedance versus frequency plots were recorded following respective depositions on the fresh electrode surface for the individual peptide–phospholipid interactions. The experimental conditions for the measurement of impedance are listed in the following. For one measurement, 1 cycle was used except when the cycle was less than 1 s, in which case, the measurement time was 1 s In order to reach steady state, 10 cycles were used except when 10 cycles lasted more than 3 s, in which case, 3 s were used. Each frequency scan took 5 min with the potential continually applied commencing with the highest frequency. These time intervals are a compromise in providing sufficient time to carry out the measurement and reaching steady state, whilst still enabling all the experiments to be done within a specified time period on one phospholipid layer without altering the structure of the layer. No significant difference in the spectra was noted when longer equilibration periods were used before each experiment. The impedance data were transformed to the complex capacitance plane and the complex capacitance axes were expressed as $\mathrm{Re}Y\,\omega^{-1}$ and $\mathrm{Im}Y\,\omega^{-1}$ respectively. This was done using an EXCEL (Microsoft) spreadsheet.

For a series RC circuit, the $\mathrm{Re}Y\,\omega^{-1}$ versus $\mathrm{Im}Y\,\omega^{-1}$ plot gives a single semi-circle for the RC element, where the capacitor has no frequency dispersion. The extrapolation of this semi-circle to the $\mathrm{Im}Y\,\omega^{-1}$ axis at low frequency gives the zero frequency capacitance (ZFC) [28–30] of the RC circuit which is therefore an empirical quantity and is the monolayer capacitance ($C$). Any additional elements to the RC semi-circle at lower frequencies will correspond to properties of the monolayer. Furthermore, if the semi-circle representing the RC element is not perfect [29], the non-ideality of the capacitor is indicated. This can be due to dielectric relaxations coupled to the RC charging process and to additional circuit elements at the interface between the capacitor and the solution resistance [29,31]. Inhomogeneities in the monolayer give rise to a low frequency relaxation of the capacitor [25,26]. This is seen as an additional capacitative element which appears to the right of the RC semi-circle in the complex capacitance plane plot [25,26]. The ZFC of the monolayer relates to the thickness of the monolayer, $d$, and the dielectric constant,$\varepsilon$, by the equation [32]:

$$C = \varepsilon_o \varepsilon / d$$

where $\varepsilon_o = 8.84\times10^{-12}$ F $m^{-1}$ and is the vacuum permittivity. The dielectric constant or number of the vacuum, $\varepsilon=1$. An increase in the capacitance of the monolayer relates either to a decrease in its thickness or an increase in its relative dielectric constant. In either case the capacitance of a monolayer is very sensitive to its structure.

In addition, the model of Whitehouse et al. [25,26] was employed, which combined dielectric theory with electrochemical circuit theory, where the data are fitted to the equation:

$$Y = \frac{1}{R + \dfrac{1}{(i\omega)^{\beta}\omega_o^{1-\beta}\left[\dfrac{C_s - C_{inf}}{1+(i\omega\tau)^{\alpha}} + C_{inf}\right]}} \quad (1)$$

In Eq. (1), $Y$ is the admittance, $R$ is equivalent to the uncompensated solution resistance ($R_u$), $C_{inf}$ is equivalent to the zero frequency capacitance ($C$) of the monolayer, $C_s - C_{inf}$ is the additional low frequency capacitative element with relaxation time constant ($\tau$), and $\alpha$ is the coefficient which represents the distribution of time constants around the most probable value of $\tau$. $\beta$ is the coefficient which characterises non-idealities at the interface between $R$ and $C$ and is equivalent to a surface roughness. The physical meanings of $\alpha$ and $\beta$ are quite different since $\alpha$ is related to the time constant of relaxation of the additional capacitative element $C_s - C_{inf}$, a bulk dielectric property and $\beta$ relates to the flow of charge from solution into both capacitative elements, $C_{inf}$ and $C_s - C_{inf}$, which is an interfacial property. $\omega_0$ is a dummy constant which corrects for units and is always set at unity. The relationship between $\alpha$ and $\beta$ and how they affect the plots in the complex capacitance plane is very clearly explained in Figure 6 of Ref [26]. Curve fitting of the data was carried out using IGOR (wavemetrics) in the same way as described previously [25,26]. In the fitting procedure the experimental $R_u$ which is equivalent to $R$ in Eq. (1) was put in as an experimental parameter and $R_u$ was determined by extrapolating the Im $Z$ versus Re $Z$ plot to the Re $Z$ axis [33].

### 2.3. Electrochemistry of $Tl^+$/Tl(Hg)

The following procedure [20,23] was taken to measure the peptide permeabilising activity to $Tl^+$ of the monolayer. Subsequent to deaeration of the electrolyte, $10^{-4}$ mol $dm^{-3}$ Tl(I) was added from the stock solution. The lipid layer was then spread on the electrolyte and transferred to the electrode. A cyclic voltammogram was recorded to check the impermeability of the deposited layer. Following addition of peptide to the electrolyte and stirring, the phospholipid layer was deposited on the electrode surface. A series of voltage pulses from −0.2 V to potentials from −0.3 to −0.7 V vs Ag/AgCl and back were

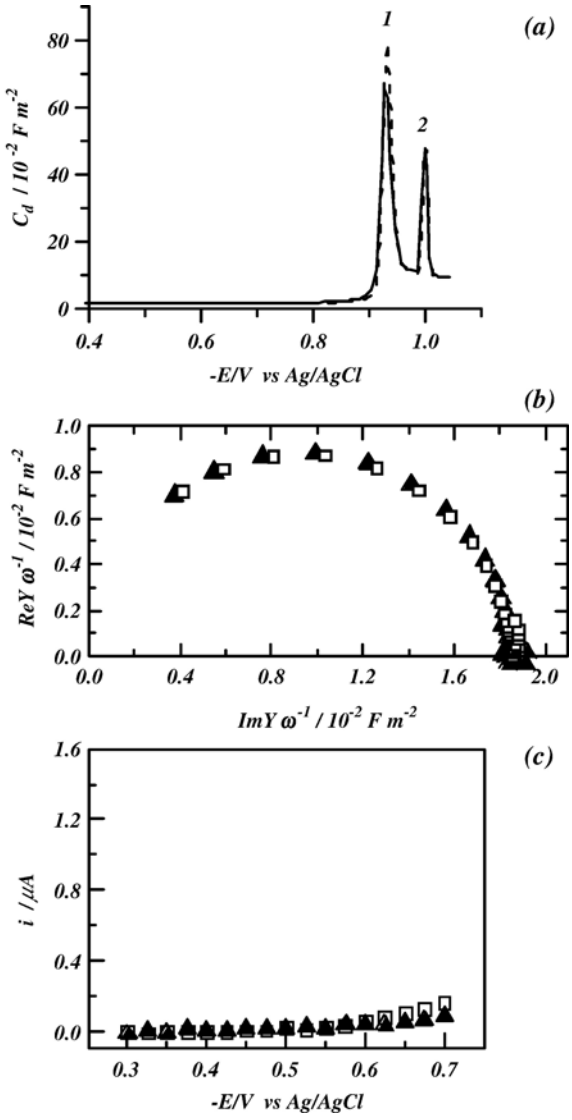


Fig. 1. (a) Capacitance–potential plots and (b) impedance plots in the complex capacity plane of, and (c) sampled current voltammetry plots of the $Tl^+$/Tl(Hg) reduction at: − DOPC coated mercury electrodes in Dulbecco's phosphate buffered saline in the absence (a, dashed line and b, c, solid triangles) and presence (a, solid line and b, c, open squares) of 9 nmol $dm^{-3}$ LL-37 peptide.

initiated and the current transients recorded. The pulses were 40 ms long and the currents were sampled at 40 kHz with a 20 kHz low pass filter. A delay period of 15 s between each pulse enabled the establishment of initial concentration conditions. After the pulsing programme had been performed, an *ac* out-of-phase voltammogram was recorded to ensure that the phospholipid layer had not degraded during the experiment. Pulse transients were analysed by sampling the current transient after a time interval of 25 ms from the beginning of the pulse and plotting this current value against potential as a sampled current voltammogram. The currents were measured for the cathodic train of pulses and the anodic train of pulses. The mean current value and the range between the two values expressed as an error bar were recorded at each potential.

In the case of $Tl^+$ reduction at the DOPC + DOPG and DOPC + lipid A coated electrodes, the entire current transient was fitted to the model describing a homogeneous chemical reaction preceding a rapid electron transfer ($C_rE_r$ mechanism). The equation characterising this model is written as [34]:

$$i(t) = \frac{FAD^{1/2}c_0}{(1-K^2)} \times \left\langle \frac{[K(e^{-kt}-K)]}{\pi^{1/2}t^{1/2}} + e^{Bt}\{\langle K(k+B)^{1/2} \times erf[(k+B)^{1/2}t^{1/2}]\rangle - B^{1/2}erf(B^{1/2}t^{1/2})\} \right\rangle \quad (2)$$

In Eq. (2), $F$ is Faraday's constant, $D$ is the diffusion coefficient and $c_0$ is the bulk concentration of $Tl^+$ and $k = k_1 + k_{-1}$ and $k_1$ and $k_{-1}$ are the forward and reverse homogeneous rate constants respectively of the chemical step of which $K(=k_1/k_{-1})$ is the

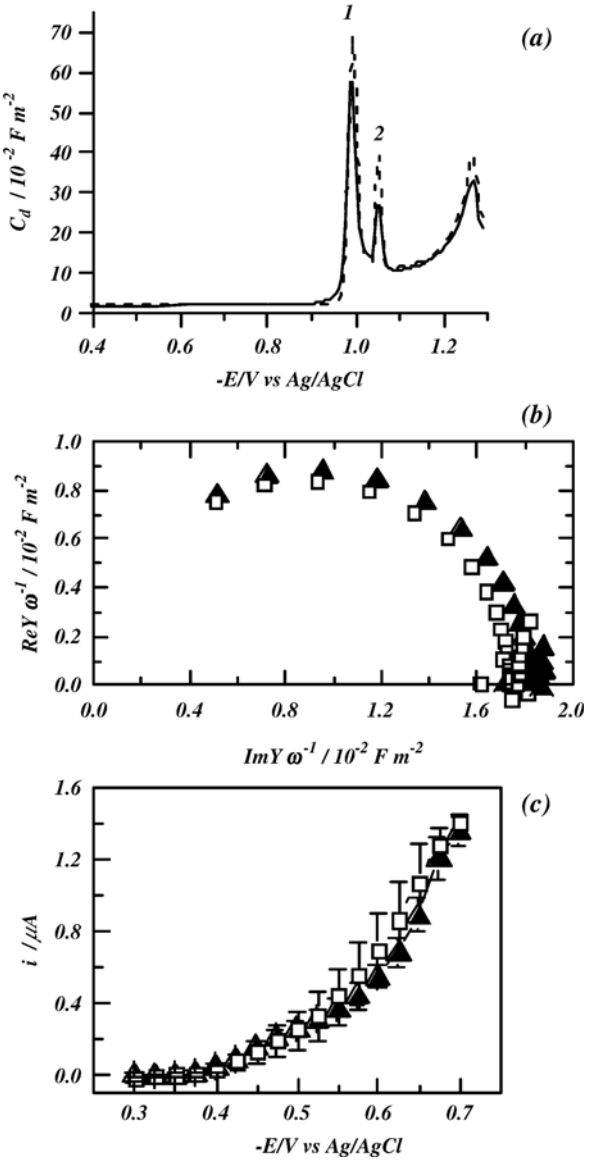


Fig. 2. (a) Capacitance–potential plots and (b) impedance plots in the complex capacity plane of, and (c) sampled current voltammetry plots of the $Tl^+$/Tl(Hg) reduction at: −50% DOPC + 50% DOPG coated mercury electrodes in Dulbecco's phosphate buffered saline in the absence (a, dashed line and b, c, solid triangles) and presence (a, solid line and b, c, open squares) of 9 nmol $dm^{-3}$ LL-37 peptide.

equilibrium constant. $k$ is a rate constant which represents the rate of attainment of chemical equilibrium prior to the charge transfer. $B=K^2k/(1-K^2)$. The important feature of Eq. (2) is that it is valid for all values of $K$ provided $k_{-1}>k_1$ and for current data obtained over all real time. This equation simplifies to the following equation at longer time scales where $k_1^{het}=Kk^{1/2}D^{1/2}$ [35] and $k_1^{het}$ is a heterogeneous rate constant describing the intrinsic monolayer permeability to $Tl^+$ at a specified potential.

$$i = FAc_0k_1^{het}\exp\left(\frac{k_1^{het^2}t}{D}\right)erfc\left(\frac{k_1^{het}t^{1/2}}{D^{1/2}}\right) \quad (3)$$

Expressed in this way, Eq. (3) is referred to as the approximate equation describing the potential step current transient resulting from the $C_rE_r$ mechanism [36]. When Eq. (2) is fitted to the current transients, the time constant ($\tau$) of the initial exponential decay corresponds to $k^{-1}$ [20,35]. Curve fitting of the data was carried out using the IGOR programme as before [20,35].

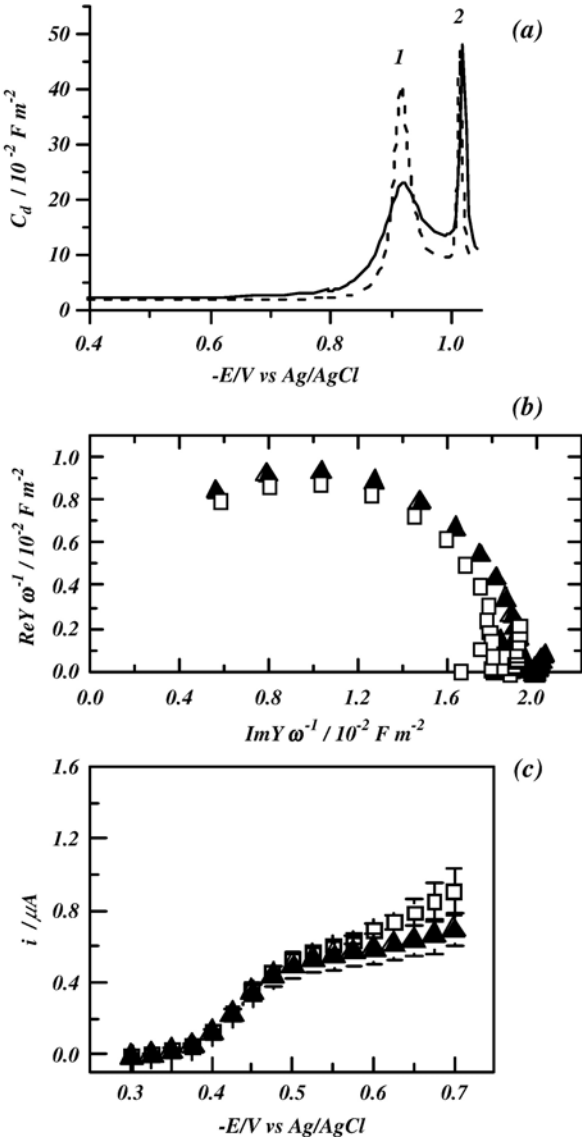


Fig. 3. (a) Capacitance–potential plots and (b) impedance plots in the complex capacity plane of, and (c) sampled current voltammetry plots of the $Tl^+$/Tl(Hg) reduction at: 70% DOPC+30% lipid A coated mercury electrodes in Dulbecco's phosphate buffered saline in the absence (a, dashed line and b, c, solid triangles) and presence (a, solid line and b, c, open squares) of 9 nmol $dm^{-3}$ LL-37 peptide.

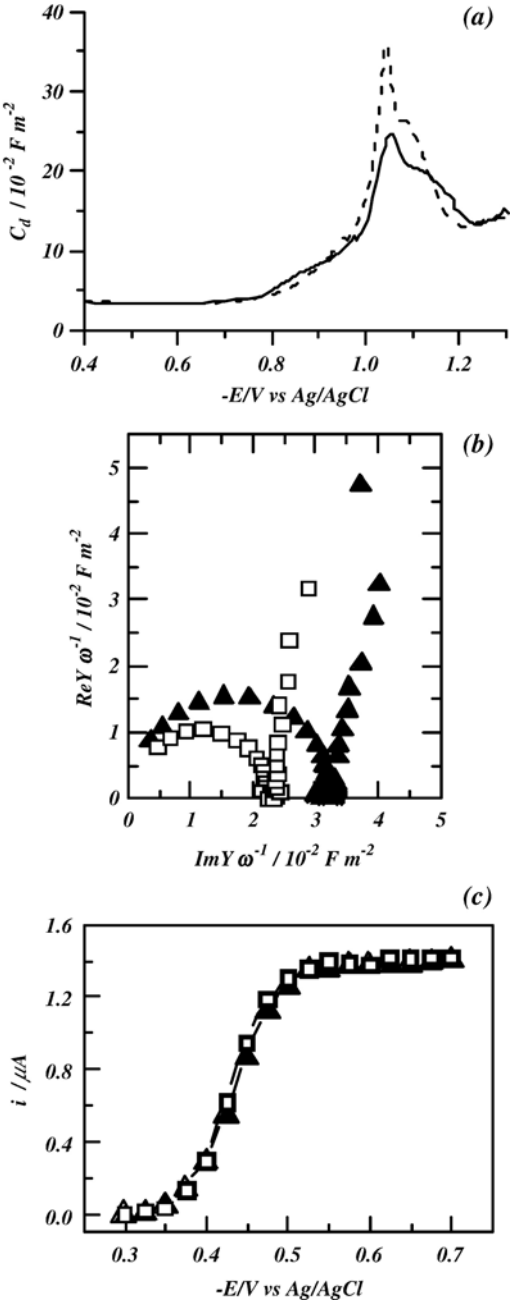


Fig. 4. (a) Capacitance–potential plots and (b) impedance plots in the complex capacity plane of, and (c) sampled current voltammetry plots of the $Tl^+$/Tl(Hg) reduction at: lipid A coated mercury electrodes in Dulbecco's phosphate buffered saline in the absence (a, dashed line and b, c, solid triangles) and presence (a, solid line and b, c, open squares) of 9 nmol $dm^{-3}$ LL-37 peptide.

## 3. Results

### 3.1. Electrochemical characteristics of phospholipids

The capacitance–potential curves, the impedance–frequency plots in the complex capacity plane and the sampled current

voltammograms of the $Tl^+$/Tl(Hg) process at DOPC monolayer coated mercury electrodes have been previously decribed in detail [26,27] and are presented as control measurements in Fig. 1.

Monolayers of DOPC+DOPG show characteristics similar to those of DOPC and are displayed in Fig. 2.

A significant difference in the capacitance–potential curves is the shift of the capacitance peaks 1 and 2 by 0.05 V to more negative potentials. In addition, the monolayer does not suppress the $Tl^+$/Tl(Hg) redox process to the same extent as DOPC. The appearance of the voltammogram exhibits a voltage dependence of the $Tl^+$ reduction current which attains the diffusion controlled value at −0.7 V vs Ag/AgCl which is 1.3 μA under these experimental conditions where the diffusion coefficient for $Tl^+$ in 0.1 NaCl is $1.8\times10^{-9}$ $m^2$ $s^{-1}$ [37].

The electrochemical measurements of DOPC+lipid A coated electrodes are displayed in Fig. 3.

Capacity-potential plots of monolayers of DOPC+lipid A display the capacitance peaks 1 and 2 characteristic of DOPC coated electrodes (Fig. 3(a)). The impedance–frequency plots transformed to the complex capacity plane show no significant extra capacitative element and the ZFC is about 0.019 F $m^{-2}$ (Fig. 3(b)). The DOPC+lipid A layer allows the $Tl^+$/Tl(Hg) redox process to take place but with a limiting current half of that for a diffusion controlled reduction of $Tl^+$ at the uncoated mercury electrode (Fig. 3(c)).

In contrast to the DOPC mixed layers, lipid A monolayers coated on mercury show substantially different electrochemical characteristics displayed in Fig. 4 and are described in the following: (i) The capacity–potential plots show two unresolved peaks at potentials −1.05 and −1.1 V vs Ag/AgCl. At more negative potentials the capacitance of the coated electrode begins to assume that of an uncoated electrode (0.17 F $m^{-2}$) indicating the desorption of the lipid (Fig. 4(a)). (ii) impedance–frequency plots transformed to the complex capacity plane show a significant extra capacitative element in addition to the RC semi-circle and a ZFC value of ~0.0325 F $m^{-2}$ (Fig. 4(b)). Fitting of Eq. (1) to this data showed that the values of $\beta$ (0.995–0.997) were lower than those observed for a DOPC monolayer on mercury (0.998) [26]. (iii) Sampled current voltammograms show no inhibition of the $Tl^+$/Tl(Hg) redox process and the current is equivalent to the diffusion controlled reduction of $Tl^+$ at an uncoated mercury electrode (Fig. 4(c)).

Where there is limited but significant $Tl^+$ reduction at the coated electrode, the $Tl^+$ reduction current transients have been fitted to Eq. (2). The transients generally conform to those expected for a $C_rE_r$ mechanism preceding the reduction as has previously been shown for $Tl^+$ reduction following transfer through gramicidin channels [20]. An example of the reduction transients at the coated electrodes is shown in Fig. 5. The transients of $Tl^+$ reduction at the DOPC+DOPG coated electrode are different to those at the DOPC+lipid A coated electrode as shown by a higher value of coefficient $k$. These transients display a shorter relaxation time ($\tau$) prior to coinciding with the transient generated by the approximate $C_rE_r$ Eq. (3), constructed from $k_1^{het}=Kk^{1/2}D^{1/2}$ [35].

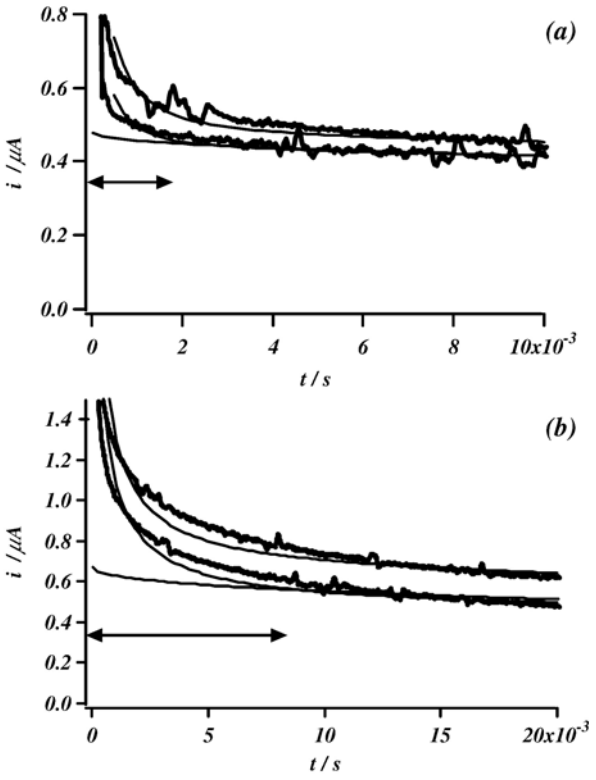


Fig. 5. Current transients due to $Tl^+$ reduction following voltage pulse from −0.2 to −0.55 V at (a) DOPC+lipid A and (b) DOPC+DOPG coated electrode. Bottom and top transients without and with 9 nmol $dm^{-3}$ LL-37 in Dulbecco's phosphate buffered saline electrolyte respectively. Thick line: data, thin solid line: fit of Eq. (2) and lowest thin solid line current generated from Eq. (3) where $k_1^{het}=Kk_{1/2}D_{1/2}$. Values of coefficients from the Eq. (3) fit as follows: (a) bottom: $K$=0.048, $k$=685 $s^{-1}$, top: $K$=0.069, $k$=416 $s^{-1}$ (b) bottom: $K$=0.18, $k$=100 $s^{-1}$, top: $K$=0.22, $k$=138 $s^{-1}$. Initial relaxation time ($\tau=1/k$) of transient indicated by double arrow.

### 3.2. Effect of LL-37 interaction with phospholipid on the impedance and permeability properties of the monolayer

Fig. 1 shows that addition of the LL-37 peptide to the electrolyte solution has no significant effect on the electrochemical characteristics of DOPC coated mercury electrodes. In comparison, Fig. 2 shows some influence on the electrochemical characteristics of the DOPC+DOPG coated electrode caused by the addition of LL-37 peptide to the electrolyte described in the following: (i) Capacitance peak 2 and the lipid desorption capacitance peak of DOPC+DOPG coated mercury are depressed to a small extent. (ii) In the impedance data plotted in the complex capacity plane, a barely significant decrease in the ZFC of DOPC+DOPG coated mercury and no introduction of an extra capacitive element is observed. (iii) The interaction of LL-37 with the DOPC+DOPG coated mercury causes a marginal increase in the $Tl^+$ reduction current.

Fig. 3 shows the following effects on the electrochemical characteristics of the DOPC+lipid A coated electrode caused by the addition of LL-37 peptide to the electrolyte: (i) Capacitance peak 1 in the capacity-potential curve is markedly suppressed. (ii) In the impedance data plotted in the complex capacity plane, a small decrease in the ZFC and no introduction of an extra capacitive element is seen. (iii) There is an increase in the $Tl^+$

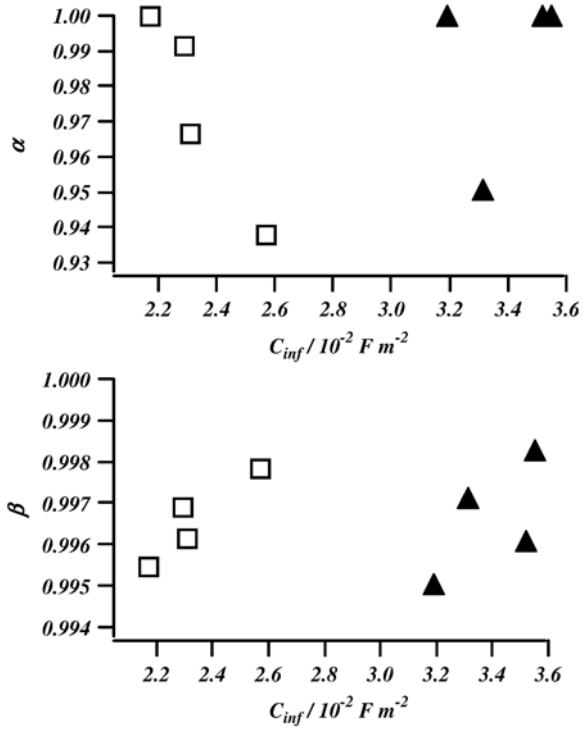


Fig. 6. Plots of coefficients $\alpha$ and $\beta$ versus $C_{inf}$ (=ZFC) extracted by fitting Eq. (1) to impedance data from lipid A coated electrodes in electrolyte (solid triangles) and lipid A coated electrodes with 9 nmol $dm^{-3}$ LL-37 in electrolyte (open squares). Errors within symbol size.

reduction current in the sampled-current voltammogram of the Tl(I)/Tl(Hg) redox process especially at more negative potentials. Finally Fig. 4 shows the following effects on the electrochemical characteristics of the lipid A coated electrode caused by the addition of LL-37 peptide to the electrolyte: (i) The capacitance peaks of the capacity-potential curve are suppressed. (ii) In the impedance data plotted in the complex capacity plane, a significant decrease in the ZFC by 30% is observed. In the series of experiments carried out, some variation in the ZFC value (0.022–0.026 F $m^{-2}$) was seen. (iii) No significant influence of LL-37 on the sampled-current voltammogram of the Tl(I)/Tl(Hg) redox process is observed which remains diffusion limited.

The current transients of $Tl^+$ reduction at the DOPC+DOPG and the DOPC+lipid A coated electrodes (see Fig. 5) show no significant difference when LL-37 is added to the electrolyte except that the currents are increased. A comparison of the relationship of $\alpha$ and $\beta$ respectively with $C_{inf}$ following the fitting of Eq. (1) to the impedance data shows that some correlation between these variables is found when applied to the experiments of the lipid A coated electrodes in the presence of LL-37 in the electrolyte. No significant correlation is seen in the absence of LL-37 in the electrolyte (see Fig. 6).

## 4. Discussion

### 4.1. Monolayer configuration

The mixed monolayers of DOPC+DOPG and DOPC+lipid A have similar properties to those of DOPC. The most important difference is the decreased suppression of the Tl(I)/Tl(Hg) redox process compared to that effected by DOPC which indicates increased permeability to $Tl^+$. This can be attributed to the presence of negative charge on the monolayer [39,40] and some mismatch between the DOPG and DOPC molecules in the monolayers of DOPC+DOPG. The absence of an extra capacitative element in the complex capacitance plots of DOPC+DOPG and DOPC+lipid A mixed monolayer coated electrodes indicates an absence of any structural inhomogeneity [25,26].

The lipid A properties on mercury show considerable departure from those of DOPC. A significant extra capacitative element indicates a structured inhomogeneous layer [25,26] and the increased value of the ZFC indicates that the layer is thinner than the DOPC layer. The decreased value of $\beta$ concurs with an increased surface roughness associated with the structured inhomogeneity [25,26]. The absence of any suppression by lipid A of the Tl(I)/Tl(Hg) redox process shows that it is permeable to $Tl^+$. The observed electrochemical data for the lipid A coated electrode concurs with the properties of lipid A [38]. Lipid A has six saturated alkyl chains four of which have 14 carbons and two with 12 carbons. This is shorter than the two alkyl chains of DOPC which have 18 carbons and accounts for the thinner layer. In addition the layer will not be fluid leading to the structured inhomogeneity. The bulky head group and overall negative charge will render the lipid A layers permeable to $Tl^+$ similar to phosphatidyl serine (PS) layers [39,40]. The lack of structural inhomogeneity in the DOPC+lipid A monolayers is also interesting and shows that the fluidity of the DOPC is dominating the monolayer.

The voltammograms of $Tl^+$ reduction at the DOPC+lipid A coated electrode are different to those at the DOPC+DOPG coated electrodes and resemble those of the gramicidin channel facilitated reduction of $Tl^+$ [20]. The lipid A could be a facilitating transport of $Tl^+$ across the mixed layer. The difference between the $Tl^+$ current transient shape characterising $Tl^+$ reduction at the DOPC+DOPG and DOPC+lipid A coated electrode is also significant (see Fig. 5). At the DOPC+lipid A coated electrode the longer relaxation time is characteristic of channel or facilitated transport by lipid A [20]. The reduction transient at the DOPC+DOPG coated electrode more nearly resembles a non specific permeability of $Tl^+$ through the layer.

### 4.2. LL-37 interaction

The small effect of the LL-37 interaction on the ZFC of the monolayers of DOPC+DOPG, DOPC+lipid A and lipid A shows that the peptide interacts selectively with the negatively charged lipids, DOPG and lipid A respectively. The significant influence of the peptide on the ZFC of a lipid A monolayer confirms this. This result is interesting since previous phospholipid interactions with peptide have shown increases in capacitance as well as the introduction of an extra capacitative element. In this instance it appears that the peptide renders the monolayer thicker shown as a decrease in capacitance. The 30% decrease in capacitance corresponds to a similar order of increase in thickness. Such an increase can only be correlated with a marked change in conformation of the layer associated with

peptide interaction. In spite of this, there is no effect on the $Tl^+$ permeability through the lipid A layer. The LL-37 interaction with the mixed DOPC+DOPG and DOPC+lipid A layers introduces no significant extra capacitative element.

The physical meaning of the correlations between the extracted parameters of the Eq. (1) fit to the impedance data from lipid A coated electrodes in electrolyte with added LL-37 (see Fig. 6) can only be speculated at this stage. If it is assumed that the decrease in $C_{inf}$ is directly related to the extent of peptide interaction with the lipid A layer, the decreased value of $\beta$ with decreased $C_{inf}$ implies that with more peptide in the layer, the layer becomes rougher. The increased value of $\alpha$ with decreased $C_{inf}$ implies that with more peptide in the layer the less diffuse is the time constant of the extra capacitative element.

These results have to be seen in context with other results obtained for LL-37 interaction with dipalmitoyl phosphatidylcholine (DPPC) monolayers at the air–water interface. Preliminary studies [41] of these interactions at the air–aqueous interface using a Langmuir trough corroborate the electrochemical findings. When lipid monolayers were held at constant pressure and LL-37 was injected under the monolayer, little interaction was seen with monolayers of DPPC shown as an insignificant increase in area per molecule. However, when LL-37 was injected under monolayers of dipalmitoyl phosphatidylglycerol (DPPG) and lipid A, a large increase in area per molecule was observed, clearly displaying interaction of the negatively charged lipids with the peptide [41].

Other work [42] has recently been published and investigates the interactions of LL-37 with simple phospholipid layers by using epifluorescence microscopy and the X-ray scattering techniques of grazing incidence X-ray diffraction and X-ray reflectivity. Epifluorescence data shows that there is very little difference in DPPC monolayer morphology after LL-37 injection, but that there are significant differences in the DPPG monolayer morphology with a large increase in disordered phase domain area after LL-37 injection. X-ray data suggests that LL-37 completely disrupts DPPG monolayers with a slight overall thinning of the monolayer most likely due to lipid reorientation. Work has also been carried out using the same X-ray techniques to observe lipid A monolayers and it appears that lipid A [43] monolayers become thicker when LL-37 is injected underneath the lipid A monolayers. This is thought to be due to the fact that the hydrocarbon chains of the lipid A molecules are quite rigid and so it is much more difficult for the peptide to penetrate the tail regions of the lipid. Therefore, the LL-37 peptide simply reaches the head region of the lipid and binds to it. This gives an overall thickening effect of the lipid A monolayer which is consistent with the impedance spectroscopy results presented in this paper.

## 5. Conclusions

The most significant finding from this study is that the LL-37 antimicrobial peptide selectively interacts with negatively charged phospholipids in particular lipid A and this interaction can be monitored using electrochemical techniques. This interaction is different from those observed previously between gramicidin [20] and synthetic self assembled peptides [44] and phospholipids in that the dielectric becomes apparently thicker associated with a significant capacitance decrease.

## Acknowledgements

Funding for this work was provided by the Joint Grant Scheme (MoD-NERC) and the EPSRC Grant Ref. GR/R67439.

## References

[1] A. Tonks, Drug resistance is a worldwide threat, warns report, British Medical Journal 309 (1994) 1109–1110.
[2] C.A. Hart, S. Kariuki, Antimicrobial resistance in developing countries, British Medical Journal 317 (1998) 647–650.
[3] J. Davies, Bacteria on the rampage, Nature 383 (1996) 219–220.
[4] M.H. Reacher, A. Shah, D.M. Livermore, M.C.J. Wale, C. Graham, A.P. Johnson, H. Heine, M.A. Monnickendam, K.F. Barker, D. James, R.C. George, Bacteraemia and antibiotic resistance of its pathogens reported in England and Wales between 1990 and 1998: trend analysis, BMJ 320 (2000) 213–216.
[5] M.A. Borg, Bed occupancy and overcrowding as determinant factors in the incidence of MRSA infections within general ward settings, Journal of Hospital Infection 54 (2003) 316–318.
[6] I. Kubo, K.-I. Fujita, K.-I. Nihei, Molecular design of multifunctional antibacterial agents against methicillin resistant *Staphylococcus aureus* (MRSA), Bioorganic and Medicinal Chemistry 11 (2003) 4255–4262.
[7] M.C. Enright, The evolution of a resistant pathogen— the case of MRSA, Current Opinion in Pharmacology 3 (2003) 474–479.
[8] M. Zasloff, Antimicrobial peptides of multicellular organisms, Nature 415 (2002) 389–395.
[9] D. Andreu, L. Rivas, Animal antimicrobial peptides: an overview, Biopolymers 47 (1998) 415–433.
[10] K. Matsuzaki, K. Sugishita, N. Fujii, K. Miyajima, Molecular-basis for membrane selectivity of an antimicrobial peptide, Magainin-2, Biochemistry 34 (1995) 3423–3429.
[11] K. Matsuzaki, Why and how are peptide–lipid interactions utilized for self-defense? Magainins and tachyplesins as archetypes, Biochimica Et Biophysica Acta 1462 (1999) 1–10.
[12] O. Konovalov, I. Myagkov, B. Struth, K. Lohner, Lipid discrimination in phospholipid monolayers by the antimicrobial frog skin peptide PGLa. A synchrotron X-ray grazing incidence and reflectivity study, European Biophysics Journal with Biophysics Letters 31 (2002) 428–437.
[13] Z. Oren, J.C. Lerman, G.H. Gudmundsson, B. Agerberth, Y. Shai, Structure and organization of the human antimicrobial peptide LL-37 in phospholipid membranes: relevance to the molecular basis for its non-cell-selective activity, Biochemical Journal 341 (1999) 501–513.
[14] K. Putsep, G. Carlsson, H.G. Boman, M. Andersson, Deficiency of antibacterial peptides in patients with Morbus Kostmann: an observation study, Lancet 360 (2002) 1144–1149.
[15] R. Bals, J.M. Wilson, Cathelicidins — a family of multifunctional antimicrobial peptides, Cellular and Molecular Life Sciences 60 (2003) 711–720.
[16] R. Bals, X.R. Wang, M. Zasloff, J.M. Wilson, The peptide antibiotic LL-37/hCAP-18 is expressed in epithelia of the human lung where it has broad antimicrobial activity at the airway surface, Proceedings of the National Academy of Sciences of the United States of America 95 (1998) 9541–9546.
[17] H.G. Boman, Antibacterial peptides: basic facts and emerging concepts, Journal of International Medicine 254 (2003) 197–215.
[18] Y. Wang, G. Walter, E. Herting, B. Agerberth, J. Johansson, Antibacterial activities of the cathelicidins prophenin (residues 62 to 79) and LL-37 in the presence of a lung surfactant preparation, Antimicrobial Agents and Chemotherapy 48 (2004) 2097–2100.
[19] D.M.E. Bowdish, D.J. Davidson, M.G. Scott, R.E.W. Hancock, Immunomodulatory activities of small host defense peptides, Antimicrobial Agents and Chemotherapy 49 (2005) 1727–1732.

[20] A. Nelson, Conducting gramicidin channel activity in phospholipid monolayers, Biophysical Journal 80 (2001) 2694–2703.
[21] B. Lindholm-Sethson, J. Nystrom, P. Geladi, A. Nelson, Gramicidin A interaction at a dioleoyl phosphatidylcholine monolayer on a mercury drop electrode, Analytical and Bioanalytical Chemistry 375 (2003) 350–355.
[22] M. Naumowicz, Z. Figaszewski, Impedance analysis of phosphatidylcholine membranes modified with gramicidin D, Bioelectrochemistry 61 (2003) 21–27.
[23] A. Nelson, Electrochemical studies of thallium(I) transport across gramicidin modified electrode-adsorbed phospholipid monolayers, Journal of Electroanalytical Chemistry 303 (1991) 221–236.
[24] M. Rueda, I. Navarro, G. Ramirez, F. Prieto, A. Nelson, Impedance measurements with phospholipid-coated mercury electrodes, Journal of Electroanalytical Chemistry 454 (1998) 155–160.
[25] C. Whitehouse, D. Gidalevitz, M. Cahuzac, R.E. Koeppe II, A. Nelson, Interaction of gramicidin derivatives with phospholipid monolayers, Langmuir 20 (2004) 9291–9298.
[26] C. Whitehouse, R. O'Flanagan, B. Lindholm-Sethson, B. Movaghar, A. Nelson, Application of electrochemical impedance spectroscopy to the study of dioleoyl phosphatidylcholine monolayers on mercury, Langmuir 20 (2004) 136.
[27] D. Bizzotto, A. Nelson, Continuing electrochemical studies of phospholipid monolayers of dioleoyl phosphatidylcholine at the mercury–electrolyte interface, Langmuir 14 (1998) 6269–6273.
[28] S. Lingler, I. Rubinstein, W. Knoll, A. Offenhausser, Fusion of small unilamellar lipid vesicles to alkanethiol and thiolipid self-assembled monolayers on gold, Langmuir 13 (1997) 7085–7091.
[29] B. Lindholm-Sethson, Electrochemistry at ultrathin organic films at planar gold electrodes, Langmuir 12 (1996) 3305–3314.
[30] L. Strašák, J. Dvořák, S. Hason, V. Vetterl, Electrochemical impedance spectroscopy of polynucleotide adsorption, Bioelectrochemistry 56 (2002) 37–41.
[31] P. Peng Diao, D. Jiang, X. Cui, D. Gu, R. Tong, B. Zhong, Studies of structural disorder of self-assembled thiol monolayers on gold by cyclic voltammetry and ac impedance, Journal of Electroanalytical Chemistry 464 (1999) 61–67.
[32] A.J. Bard, L.R. Faulkner, Electrochemical Methods: Fundamentals and Applications, John Wiley, New York, 1980, pp. 500–501.
[33] R.P. Janek, W.R. Fawcett, A. Ulman, Impedance spectroscopy of self-assembled monolayers on Au(111): evidence for complex double-layer structure in aqueous $NaClO_4$ at the potential of zero charge, Journal of Physical Chemistry. B 101 (1997) 8550–8558.
[34] D.D. Macdonald, Transient Techniques in Electrochemistry, Plenum Press, New York, 1977, pp. 96–100.
[35] A. Nelson, D. Bizzotto, Chronoamperometric study of Tl(I) reduction at gramicidin-modified phospholipid-coated mercury electrodes, Langmuir 15 (1999) 7031–7039.
[36] Z. Galus, Fundamentals of Electrochemical Analysis, 1st edition, Ellis Horwood, Chichester, UK, 1977, pp. 335–386.
[37] J. Koryta, J. Dvorak, Principles of Electrochemistry, John Wiley, Chichester, 1987, p. 128.
[38] A. El-Aneed, J. Banoub, Elucidation of the molecular structure of lipid A isolated from both a rough mutant and a wild strain of *Aeromonas salmonicida* lipopolysaccharides using electrospray ionization quadrupole time-of-flight tandem mass spectrometry, Rapid Communications in Mass Spectrometry 19 (2005) 1683–1695.
[39] A. Nelson, Voltammetry of Tl(I), Cd(II), Cu(II), Pb(II) and Eu(III) at phosphatidylserine-coated mercury-electrodes, Journal of the Chemical Society. Faraday Transactions 89 (1993) 3081–3090.
[40] L.A. Meijer, F.A.M. Leermakers, A. Nelson, Modelling of the electrolyte ion phospholipid layer interaction, Langmuir 10 (1994) 1199–1206.
[41] F. Neville, M. Cahuzac, A. Nelson, D. Gidalevitz, The interaction of antimicrobial peptide LL-37 with artificial biomembranes: epifluorescence and impedance spectroscopy approach, Journal of Physics. Condensed Matter 16 (2004) S2413–S2420.
[42] F. Neville, M. Cahuzac, O. Konovalov, Y. Ishitsuka, K.Y.C. Lee, I. Kuzmenko, G.M. Kale, D. Gidalevitz, Lipid headgroup discrimination by antimicrobial peptide LL-37: insight into mechanism of action, Biophysical Journal 90 (2006) 1275–1287.
[43] F. Neville, C.S. Hodges, C. Liu, O. Konovalov, D. Gidalevitz, In-situ characterization of lipid A interaction with antimicrobial peptides using surface X-ray scattering, Biophysica et Biochimica Acta: Biomembranes 1758 (2006) 232–240.
[44] E. Protopapa, A. Aggeli, N. Boden, P.F. Knowles, L.C. Salay, A. Nelson, in press. Electrochemical screening of self-assembling β-sheet peptides using supported phospholipid monolayers, Medical Engineering and Physics.